JCI The Journal of Clinical Investigation

Muscle-specific 4E-BP1 signaling activation improves metabolic parameters during aging and obesity

Shihyin Tsai, … , Albert R. La Spada, Brian K. Kennedy

J Clin Invest. 2015;125(8):2952-2964. https://doi.org/10.1172/JCI77361.

Research Article **Metabolism**

Eukaryotic translation initiation factor 4E–binding protein 1 (4E-BP1) is a key downstream effector of mTOR complex 1 (mTORC1) that represses cap-dependent mRNA translation initiation by sequestering the translation initiation factor eIF4E. Reduced mTORC1 signaling is associated with life span extension and improved metabolic homeostasis, yet the downstream targets that mediate these benefits are unclear. Here, we demonstrated that enhanced 4E-BP1 activity in mouse skeletal muscle protects against age- and diet-induced insulin resistance and metabolic rate decline. Transgenic animals displayed increased energy expenditure; altered adipose tissue distribution, including reduced white adipose accumulation and preserved brown adipose mass; and were protected from hepatic steatosis. Skeletal muscle–specific 4E-BP1 mediated metabolic protection directly through increased translation of peroxisome proliferator–activated receptor γ coactivator-1α (PGC-1α) and enhanced respiratory function. Non–cell autonomous protection was through preservation of brown adipose tissue metabolism, which was increased in 4E-BP1 transgenic animals during normal aging and in a response to diet-induced type 2 diabetes. Adipose phenotypes may derive from enhanced skeletal muscle expression and secretion of the known myokine FGF21. Unlike skeletal muscle, enhanced adipose-specific 4E-BP1 activity was not protective but instead was deleterious in response to the same challenges. These findings indicate that regulation of 4E-BP1 in skeletal muscle may serve as an important conduit through which mTORC1 controls metabolism.

Muscle-specific 4E-BP1 signaling activation improves metabolic parameters during aging and obesity

Shihyin Tsai,[1] Joanna M. Sitzmann,[1] Somasish G. Dastidar,[2] Ariana A. Rodriguez,[1] Stephanie L. Vu,[1] Circe E. McDonald,[1] Emmeline C. Academia,[1] Monique N. O'Leary,[1] Travis D. Ashe,[2] Albert R. La Spada,[2,3] and Brian K. Kennedy[1]

[1]Buck Institute for Research on Aging, Novato, California, USA. [2]Departments of Pediatrics, Cellular and Molecular Medicine, and Neuroscience, Division of Biological Sciences, Institute for Genomic Medicine, and Sanford Consortium for Regenerative Medicine, University of California, San Diego, La Jolla, California, USA. [3]Rady Children's Hospital, San Diego, California, USA.

Eukaryotic translation initiation factor 4E–binding protein 1 (4E-BP1) is a key downstream effector of mTOR complex 1 (mTORC1) that represses cap-dependent mRNA translation initiation by sequestering the translation initiation factor eIF4E. Reduced mTORC1 signaling is associated with life span extension and improved metabolic homeostasis, yet the downstream targets that mediate these benefits are unclear. Here, we demonstrated that enhanced 4E-BP1 activity in mouse skeletal muscle protects against age- and diet-induced insulin resistance and metabolic rate decline. Transgenic animals displayed increased energy expenditure; altered adipose tissue distribution, including reduced white adipose accumulation and preserved brown adipose mass; and were protected from hepatic steatosis. Skeletal muscle–specific 4E-BP1 mediated metabolic protection directly through increased translation of peroxisome proliferator–activated receptor γ coactivator-1α (PGC-1α) and enhanced respiratory function. Non–cell autonomous protection was through preservation of brown adipose tissue metabolism, which was increased in 4E-BP1 transgenic animals during normal aging and in a response to diet-induced type 2 diabetes. Adipose phenotypes may derive from enhanced skeletal muscle expression and secretion of the known myokine FGF21. Unlike skeletal muscle, enhanced adipose-specific 4E-BP1 activity was not protective but instead was deleterious in response to the same challenges. These findings indicate that regulation of 4E-BP1 in skeletal muscle may serve as an important conduit through which mTORC1 controls metabolism.

Introduction

mTOR complex 1 (mTORC1) is a principal cellular sensor of nutrient availability that, in turn, regulates cellular growth and proliferation. Activated mTORC1 signaling is associated with increased nutrient uptake and decreased autophagy, which are often seen in many cancers and metabolic disorders such as type 2 diabetes. Conversely, reduced mTORC1 activity, by caloric restriction, rapamycin treatment, or genetic manipulation, extends life span and likely health span in many model organisms (1–5). However, the relevant downstream substrates and key tissues by which reduced mTORC1 signaling provides these benefits remain to be determined.

Two key downstream substrates of the mTORC1 complex, S6 kinase (S6K) and eukaryotic translation initiation factor 4E–binding protein (4E-BP), have been linked to longevity in invertebrates (4). mTORC1 phosphorylation of S6K leads to its activation, whereas phosphorylation of 4E-BP inhibits its ability to sequester eIF4E (6–8). Although reduced S6K signaling increases energy expenditure and extends life span in mice (8–10), the fate of mice with activated 4E-BP is currently unknown.

In addition, the specific tissue(s) in which mTORC1 inactivation mediates longevity and improved metabolic homeostasis has not been determined. Adipose tissue is a prime candidate, since tissue-specific inactivation of the mTORC1 component *Rptor* in this tissue promotes reduced adiposity and subsequently protects against metabolic stress (11). Skeletal muscle is another candidate for mediating the metabolic protection afforded by reduced mTORC1 signaling, particularly given that activation of the *Drosophila* equivalent of *4E-BP* (*d4E-BP*) specifically in muscle suppresses age-related tissue degeneration and is sufficient to enhance life span in the fly (12). mTORC1 activity is crucial during muscle development, as modulations that blunt mTORC1 activity cause muscular dystrophy, while enhanced mTORC1 activity is required for muscle hypertrophy and recovery from injury (13–17). However, sustained activation of mTORC1 in aging animals results in severe myopathy (18, 19), suggesting that the effects of mTORC1 activation are tightly regulated and coordinated in skeletal muscle, with proper levels of mTORC1 activity important for both response to injury and long-term tissue function in aging animals.

Skeletal muscle and adipose tissue share a number of intrinsic functions in the regulation of energy homeostasis. First, they are both derived from the same mesenchymal stem cells, with brown adipocytes in particular sharing a common precursor cell with skeletal muscle cells (20). Second, muscle and adipose tissue are both major sites of thermogenesis, oxidizing fatty acids and dissipating energy as heat via the action of uncoupling proteins (21). Third, both tissues exhibit plasticity, adapting to either oxidative or glycolytic metabolism as their main energy source, as needed (22–24). Finally, genetic reprogramming of transcription factors involved in mitochondrial biogenesis leads to muscle fiber transformation or a white fat–to–brown fat phenotypic switch, which is ultimately correlated with an alternation in energy expenditure (24–27).

Conflict of interest: The authors have declared that no conflict of interest exists.
Submitted: June 5, 2014; **Accepted:** May 26, 2015.
Reference information: *J Clin Invest*. 2015;125(8):2952–2964. doi:10.1172/JCI77361.

Mice lacking *4e-bp1* have a significant reduction of adipose tissue and an increase in whole-body energy expenditure, while mice lacking both *4e-bp1* and *4e-bp2* reverse this phenomenon (28), suggesting that the tissue-specific effect mediated by different 4E-BP family members in the regulation of metabolic homeostasis might be masked in whole-body knockout mice. To elucidate the factors downstream of mTORC1 signaling that systemically coordinate energy homeostasis in vivo, we generated transgenic mice overexpressing a constitutively active, mTORC1-nonresponsive form of 4E-BP1 (29) in either skeletal muscle or adipose tissue. We demonstrate that enhanced 4E-BP1 activity in skeletal muscle leads to increased oxidative metabolism and protects mice from diet- and age-induced whole-body metabolic dysfunction. In contrast, activated 4E-BP1 in adipose tissue sensitized mice to diet-induced obesity with insulin resistance.

Results

Muscle 4E-BP1 non–cell autonomously regulates adipose tissue homeostasis. To test the role of mTORC1-dependent regulation of 4E-BP1 in energy homeostasis, we generated *4E-BP1* transgenic mice with mTOR phosphorylation site mutations (threonine to alanine at amino acid positions 37 and 46; *Tg-4EBP1mt* mice) to yield a constitutively active form of the protein (ref. 29 and Supplemental Figure 1A; supplemental material available online with this article; doi:10.1172/JCI77361DS1). The expression of the transgene is repressed by a *loxP*-flanked STOP codon cassette. Tissue-specific expression of CRE excises the repressive element and permits expression from the potent *CAGGS* promoter-enhancer. Therefore, we could study both cell-autonomous and non–cell autonomous mechanisms of 4E-BP1 activities regulated by mTORC1 dependency in whole-body energy homeostasis.

The CRE recombinase enzyme under the control of the mouse *Fabp4* promoter (*Fabp4-Cre*) or the muscle creatine kinase promoter (*Ckmm-Cre*) was used to selectively induce transgenic *4E-BP1* expression in mouse adipose tissue or skeletal muscle (refs. 30, 31, and Supplemental Figure 1, B–D). For simplicity, we refer to these mice as *Tg-4EBP1mt-fat* and *Tg-4EBP1mt-muscle* mice, respectively. Both *Fabp4-Cre* and *Ckmm-Cre* are expressed at a late stage of adipose and skeletal muscle differentiation; thus, we could study the role of 4E-BP1 in the maintenance of mature adipocytes and skeletal muscle fibers and determine how the genetically modified target tissues regulate whole-body energy expenditure. Both mouse lines yielded viable and fertile mice.

In transgenic mice, in which 4E-BP1mt protein is overexpressed, 4E-BP1 migrated faster than endogenous mouse 4E-BP1, which we attribute to mTORC1 nonresponsiveness (Supplemental Figure 1, B and D). Transgenic 4E-BP1mt protein showed increased binding to eIF4E, which in turn reduced eIF4E association with eIF4G (Supplemental Figure 2, A–D). Global protein translation was not altered in 4E-BP1–activated skeletal muscle (Supplemental Figure 2, E–G), suggesting that cap-independent translation control is compensatory. This is consistent with prior observations in an independent *4E-BP1* transgenic mouse line in which acute activation of 4E-BP1 in normal thymocytes did not impede global protein translation (32). In contrast, acute activation of 4E-BP1 in AKT-induced T cell lymphoma markedly reduced protein translation (32).

Notably, endogenous 4E-BP1 expression was upregulated in *Tg-4EBP1mt-muscle* mouse skeletal muscle (Supplemental Figure 1, B and E). *d4E-BP* is a known dFOXO target in *Drosophila* (12, 33). In addition, we detected induction of FOXO1 expression at both the protein and mRNA levels (Supplemental Figure 3). This suggests positive feedback regulation, with 4E-BP1 promoting FOXO1 expression, which in turn leads to enhanced transcription of *4e-bp1* mRNA.

While both groups of *4E-BP1* double-transgenic mice developed normally, we found that *Tg-4EBP1mt-muscle* mice exhibited reduced body weight (Figure 1A and Supplemental Figure 4A). At 2 months of age, *Tg-4EBP1mt-muscle* mice weighed significantly less than control mice (19% less for males and 17% less for females). The difference was not a result of feeding (Supplemental Figure 4, B and C), and we did not detect a difference in IGF-1 or growth hormone levels (Supplemental Figure 4D and data not shown), suggesting that changes in hormone levels do not underlie the small body size of *Tg-4EBP1mt-muscle* mice. Correlated with the decrease in body weight, there was a reduced lean body mass in *Tg-4EBP1mt-muscle* mice (Figure 1B). Moreover, male *Tg-4EBP1mt-muscle* mice had significantly lower plasma glucose levels than control mice (152 ± 18.0 mg/dl versus 173 ± 25.4 mg/dl, respectively) (Supplemental Figure 5A). Nonetheless, *Tg-4EBP-1mt-muscle* mice exhibited comparable glucose homeostasis to control mice, including a normal insulin response and glucose clearance rate on a normal chow diet (Supplemental Figure 5, B–E). There was also a slight reduction in body weight for male *Tg-4EBP1mt-fat* mice, coupled to increased insulin sensitivity and glucose tolerance (Figure 1A, Supplemental Figure 4A, and Supplemental Figure 5). Next, we examined the quantity and quality of adipose tissue in *4E-BP1* double-transgenic mice. The major fat pads, including visceral fat surrounding reproductive organs, inguinal fat, and brown fat on the shoulder, all exhibited no difference in weight when normalized to body weight in both groups of *4E-BP1* double-transgenic mice (Supplemental Figure 6). Histological analysis of white adipose tissue from *Tg-4EBP1mt-muscle* mice revealed a marked reduction in cell size and a decrease of subcutaneous fat deposits under the skin, whereas there was no effect in *Tg-4EBP1mt-fat* mice (data not shown). The reduction of cell size in *Tg-4EBP1mt-muscle* mice was restricted to white adipose tissue, as brown adipose tissue was not affected (Figure 1, C and D; Supplemental Figure 7; and see below). Previously, transgenic mice with whole-body knockout of *4E-BP1* were reported to undergo a white-to-brown adipose transition, generating beige fat (24). Notably, we detected an induction of *Pgc1a* transcription in *Tg-4EBP1mt-muscle* mouse inguinal fat (Supplemental Figure 8A); however, we did not observe either multilocular adipocytes (Figure 1D) or enhanced UCP1 expression in visceral and inguinal fat pads (Supplemental Figure 8B). Moreover, expression of the peroxisome proliferator–activated receptor γ coactivator-1α (PGC-1α) target *Fndc5*, which is secreted from PGC-1α–overexpressing skeletal muscle and controls white adipose transformation (34), did not change in 4E-BP1–activated skeletal muscle (Supplemental Figure 17A). Of note, we observed increased expression of UCP1 and CPT1α in *Tg-4EBP1mt-muscle* mouse brown adipose tissue, which might contribute to their increased metabolic rate, as discussed below (Supplemental Figure 8C and Figure 2D). Taken

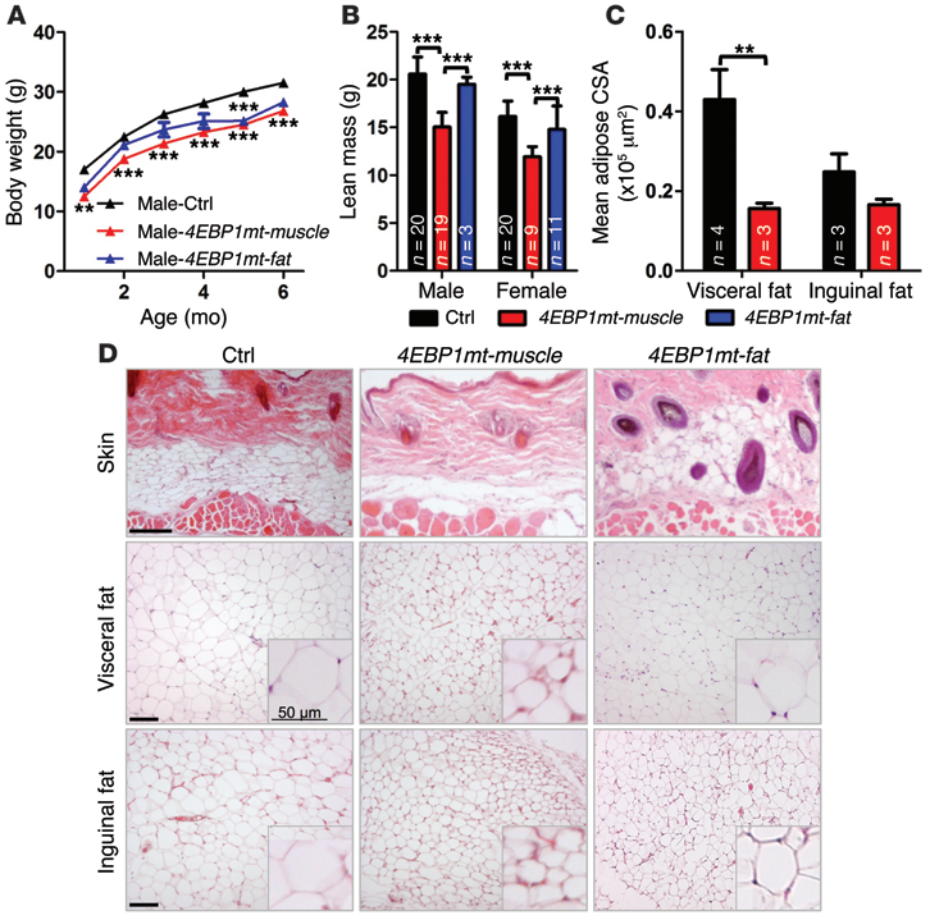

Figure 1. Activation of 4E-BP1 in mouse skeletal muscle leads to reduced body weight and atrophic white adipose tissue. (**A**) Body weight measurement in male mice (n = 8–20 per genotype). (**B**) Lean mass measurement in 2-month-old mice. (**C**) Analysis of the mean adipose cell cross-section area (CSA). (**B** and **C**) The number of mice analyzed is indicated in bars. (**D**) Representative images of hematoxylin and eosin–stained male white adipose tissue sections from skin, visceral fat, and inguinal fat of *4E-BP1* double-transgenic mice fed a normal chow diet. Scale bar: 100 μm; 50 μm (insets). P values were assessed by 2-way ANOVA. Bonferroni post-tests were used to compare replicate means by row. $^{**}P < 0.01$; $^{***}P < 0.001$.

together, these data demonstrate that adipose-specific induction of 4E-BP1 does not alter the intrinsic characteristics of adipose tissue, while skeletal muscle–specific activation of 4E-BP1 non–cell autonomously leads to white adipose atrophy.

Activation of 4E-BP1 in skeletal muscle results in muscle fiber transformation and enhanced mitochondrial respiration. Next, we characterized the cell-autonomous effect of 4E-BP1 activity in skeletal muscle. Quantitative magnetic resonance showed a decrease in lean mass proportional to reduced body weight in *Tg-4EBP1mt-muscle* mice (Supplemental Figure 9). This finding is consistent with our observation of reduced muscle fiber size and a small but detectable increase in the frequency of central nuclei in *Tg-4EBP1mt-muscle* mouse skeletal muscle (Supplemental Figure 10). Since enhanced expression of autophagy genes is associated with muscle atrophy and these genes are known targets of FOXO1 (35, 36), we examined their expression. Of the 6 genes tested, 4 exhibited significantly increased expression. Furthermore, we detected increased levels of the autophagic marker LC3-II isoform (Supplemental Figure 11). *Tg-4EBP1mt-muscle* mice showed a reduced running capacity on the treadmill (Supplemental Figure 12, A and B); however, voluntary home cage activity was not affected (Supplemental Figure 12, C and D).

Despite these observations, *Tg-4EBP1mt-muscle* mouse skeletal muscle did not exhibit fibrosis, characteristic of muscular dystrophy, or abnormal glycogen deposition (Supplemental Figure 10A), which was observed in the skeletal muscle–specific *Rptor* knockout mice (17). The differences between skeletal muscle *Rptor* knockout mice and *Tg-4EBP1mt-muscle* mice are somewhat surprising, since (a) reduced mTORC1 signaling should lead to enhanced 4E-BP1 function and (b) both mutants have elevated FOXO1 expression. Mice with skeletal muscle lacking *Rptor* or overexpressing *Foxo1* have both impaired insulin signaling and glucose homeostasis (17, 37). However, *Tg-4EBP1mt-muscle* mice had comparable glucose metabolism to that of control mice and upregulated AKT1 expression in skeletal muscle (Supplemental Figure 5 and Supplemental Figure 13A). Increased AKT1 levels may better attenuate the effects of enhanced FOXO1, thereby allowing mice to maintain normal glucose homeostasis. For instance, upon insulin activation, we observed a proportional increase of phosphorylated FOXO1 relative to total protein (data not shown). In addition, there was differential expression of FOXO1 target genes in skeletal muscle of *Tg-4EBP1mt-muscle* mice. While atrophy, autophagy, and gluconeogenesis-associated genes were induced, we did not detect enhanced expression of genes encoding cell cycle, oxidative stress, or DNA repair components (Supplemental Figure 13B). These results demonstrate that, unlike inactivation of *Rptor* in skeletal muscle, which causes progressive dystrophy, transgenic activation of 4E-BP1 in mouse skeletal muscle results in atrophic muscle and attenuates physical performance, while maintaining normal glucose homeostasis and metabolism.

In skeletal muscle histological sections, we observed an increase of intramuscular fat in *Tg-4EBP1mt-muscle* mice (Supplemental Figure 10A). Using quantitative magnetic resonance, we

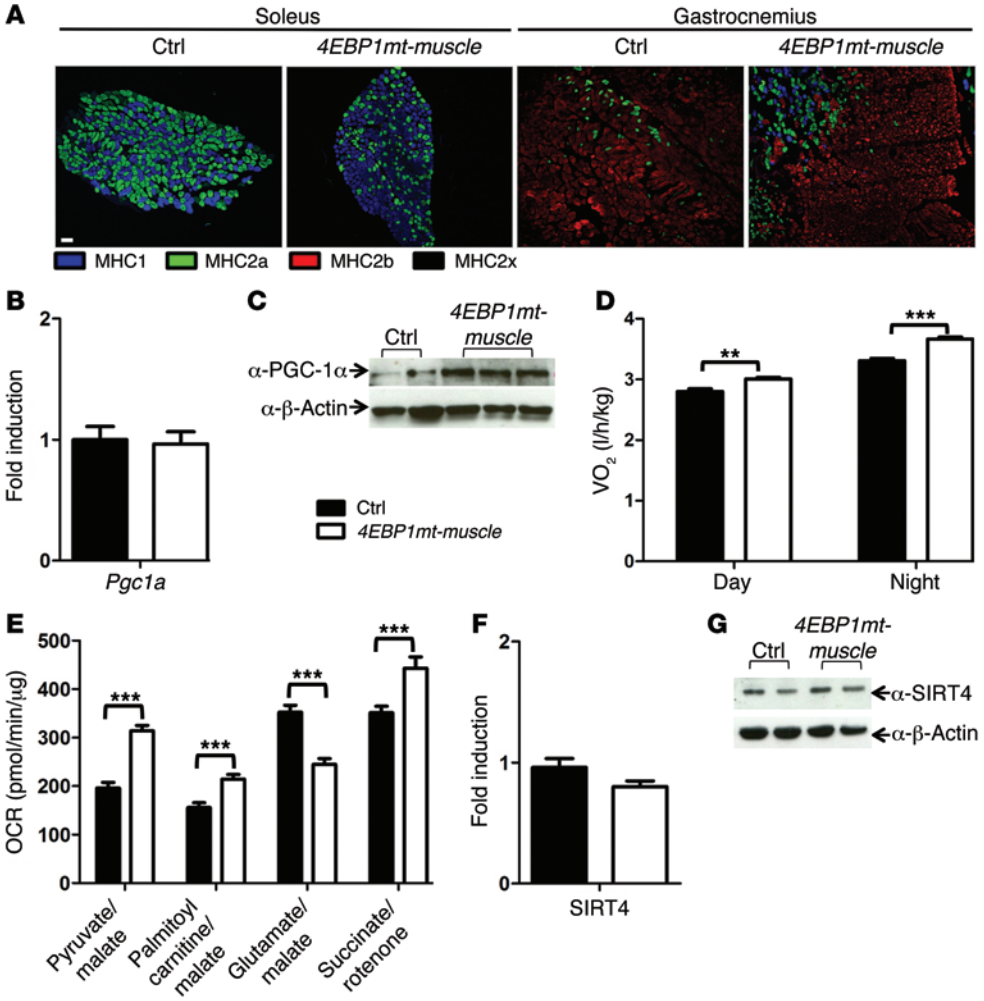

Figure 2. *Tg-4EBP1mt-muscle* mice exhibit muscle type transformation and increased oxygen consumption. (**A**) Immunofluorescence staining of type I skeletal muscle fibers (MHCI, blue) and type II skeletal muscle fibers (MHC2a, green; MHC2b, red; and MHC2x, unstained). Scale bar: 100 μm. (**B**) RT-PCR quantification of *Pgc1a* expression in quadriceps normalized to *Ppia* expression (n = 4). (**C**) Western blot analysis of PGC-1α expression in quadriceps. (**D**) Oxygen consumption measured in a 3-day/night period in 6-month-old male mice fed a normal chow diet (n = 8–12 per genotype). (**E**) State III oxygen consumption rates (OCRs) from isolated skeletal muscle mitochondria in the presence of indicated substrates were measured in an XF24 Extracellular Flux Analyzer (n = 5 per genotype). (**F**) RT-PCR and (**G**) Western blot analysis of SIRT4 expression in quadriceps. P values were assessed by a 2-way ANOVA. Bonferroni post-tests were used to compare replicate means by row. $^{**}P < 0.01$; $^{***}P < 0.001$. RT-PCR samples were from n = 4 per genotype.

also detected an increase in whole-body fat, which may be attributable to the skeletal muscle phenotype (Supplemental Figure 6B and Supplemental Figure 14). This is surprising since accumulation of intramuscular fat, at least coupled to increased white adipose tissue mass and higher serum-free fatty acid levels, is highly correlated with insulin resistance and the development of type 2 diabetes. However, calorie restriction and exercise also lead to an increase of intramuscular fat, with a reduction in white adipose tissue and normal levels of serum-free fatty acids (38–42). Furthermore, athletes or calorie-restricted model organisms are insulin sensitive, having higher metabolic rates and extended health span. Consistent with the latter scenario *Tg-4EBP1mt-muscle* mice had comparable basal leptin and glucose levels and serum lipid profiles and, more importantly, retained insulin sensitivity (Supplemental Figure 5, Supplemental Figure 14C, and Supplemental Figure 15).

There are 4 defined muscle types characterized in mammals. Type I, type IIa, and type IIx predominantly use oxidative respiration for energy production, while type IIb mainly uses glycolysis (43, 44). Overexpression of AKT1 in skeletal muscle causes muscle hypertrophy and increased type IIb muscle (glycolytic) fibers (15). Even though there was an induction of AKT1 expression in *Tg-4EBP1mt-muscle* mouse skeletal muscle, immunofluorescence revealed an increase of oxidative muscle, a finding confirmed by enhanced troponin I (slow) and *MhcI* expression (Figure 2A and Supplemental Figure 16). Moreover, protein levels of PGC-1α, which regulates mitochondrial biogenesis (45, 46), were enhanced even though mRNA levels were not altered (Figure 2, B and C). We speculate that activation of 4E-BP1 promotes PGC-1α translation. There was also a differential enhancement of PGC-1α target genes in 4E-BP1–activated skeletal muscle (Supplemental Figure 17). The fact that some but not all target genes were induced may reflect differential expression of transcription factors coactivated by PGC-1α.

There was a marked increase in mitochondrial DNA copy number as well as enhanced whole-body oxygen consumption and energy expenditure in *Tg-4EBP1mt-muscle* mice, which correlated with increased oxidative muscle fibers (Figure 2D, Supplemental Figure 16E, and Supplemental Figure 18A). Consistently, mitochondrial oxygen consumption rates measured in isolated skeletal muscle mitochondria were both high in ADP-stimulated respiration (state III) and maximal uncoupled respiration (FCCP) (Figure 2E and Supplemental Figure 18, C and D). Interestingly, state III respiration rates of *Tg-4EBP1mt-muscle* mouse mitochondria were enhanced with a lipid substrate (palmitoyl-CoA plus carnitine) and carbohydrate substrates (pyruvate and succinate), but they were selectively reduced with glutamate. A similar phenomenon has been observed in rapamycin-treated wild-type mice (47). mTORC1 has been linked to enhanced glutamine metabolism via suppres-

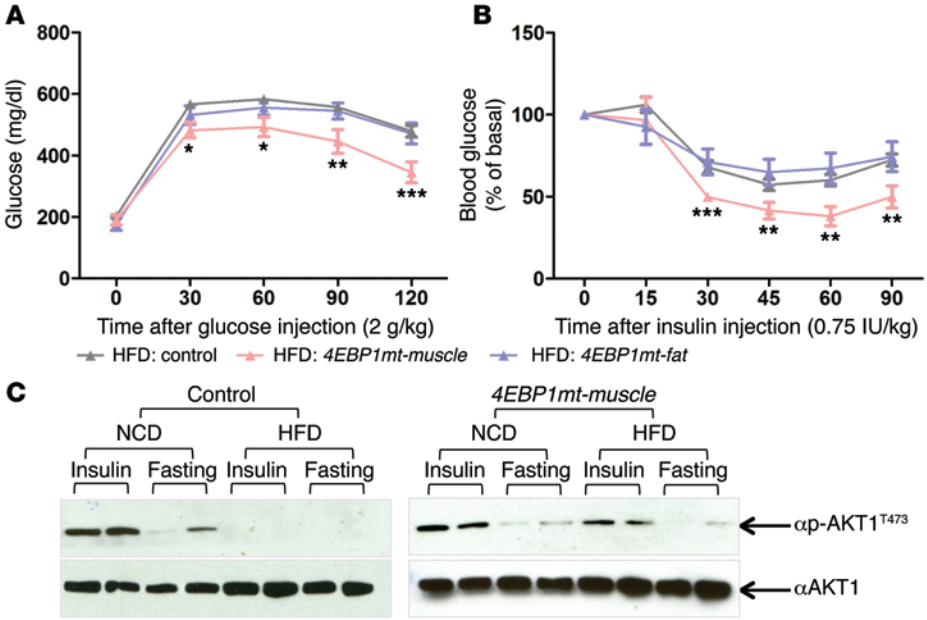

Figure 3. *Tg-4EBP1mt-muscle* mice preserve insulin sensitivity in HFD-induced type 2 diabetes mouse model. (**A**) Glucose tolerance assay and (**B**) insulin challenge assay in 6-hour–fasted males fed a HFD at 6 months of age (n = 8–24 per genotype). (**C**) Immunoblotting of AKT1 phosphorylation at Ser 473 and total AKT1 detected in skeletal muscle of male mice before (–) or after (+) insulin stimulation on a normal chow diet or HFD. P values were calculated by 1-tailed unpaired Student's t test. $^{*}P < 0.05$; $^{**}P < 0.01$; $^{***}P < 0.001$.

sion of SIRT4 in cancer cells (48). Therefore, we checked the expression of SIRT4 but did not find any change (Figure 2, F and G). Moreover, *Tg-4EBP1mt-muscle* mice have comparable respiratory quotient (RQ) values, as quantified by oxygen consumption and CO_2 generation, and a similar circadian transition to those of control littermates (Supplemental Figure 18B). Taken together, these results indicate that activation of 4E-BP1 in skeletal muscle directly contributes to increased oxidative metabolism in mouse skeletal muscle and leads to white adipose tissue atrophy, which consequently enhances whole-body energy expenditure.

Tg-4EBP1mt-muscle mice are protected from diet-induced insulin resistance and lipid dysfunction. Since there is altered fat distribution in *Tg-4EBP1mt-muscle* mice on normal chow, we next examined their behavior in response to a high-fat diet (HFD) challenge. Although the weight accumulation in *Tg-4EBP1mt-muscle* mice was similar to that in littermate controls in response to overnutrition (Supplemental Figure 19), the basal glucose levels were significantly lower and the glucose clearance rate was improved (basal level of glucose: 200 ± 29.8 mg/dl versus 221 ± 27.1 mg/dl in males and 155 ± 20 mg/dl versus 172 ± 23.5 mg/dl in females) (Figure 3A and Supplemental Figure 20). Moreover, *Tg-4EBP1mt-muscle* mice maintained insulin sensitivity (Figure 3, B and C; Supplemental Figure 20D; and Supplemental Figure 21). *Tg-4EBP1mt-muscle* mice exhibited comparable insulin levels to control mice on a HFD (Supplemental Figure 20C), and they remain sensitive to insulin signaling, which likely can be attributed to increased total AKT expression in skeletal muscle (Supplemental Figure 13A). Conversely, adipose tissue–specific activation of 4E-BP1 sensitized female mice to HFD, leading to increased weight gain and more severely impaired glucose tolerance (Figure 3, Supplemental Figure 19, and Supplemental Figure 20).

Next, we examined whether improved glucose homeostasis in *Tg-4EBP1mt-muscle* mice correlated with improved fat metabolism. We found that *Tg-4EBP1mt-muscle* mice gained more fat than control mice on a HFD (Supplemental Figure 22). However, upon HFD feeding, littermate control mice exhibited elevated serum cholesterol and triglycerides, whereas *Tg-4EBP1mt-muscle* mice maintained their lipids at lower levels that were comparable to those of animals on normal chow (Figure 4, A and B). Moreover, mice placed on a HFD exhibit white adipocyte infiltration into brown adipose tissue (49, 50). We found that brown adipose tissue of *Tg-4EBP1mt-muscle* mice was preserved and that the expression of brown adipose *Ucp1* was comparably higher than that in controls on the HFD regimen (Figure 4C and Supplemental Figure 23).

As described above, *Tg-4EBP1mt-muscle* mice have improved serum lipid profiles on a HFD. The HFD often induces abnormal accumulation of triglyceride in the liver (steatosis), which further deteriorates fat metabolism. We examined the livers of *4E-BP1* double-transgenic and control mice by Oil red O staining to detect lipid accumulation. Histological analysis of *Tg-4EBP1mt-muscle* mouse liver clearly revealed marked protection against hepatic steatosis (Figure 4D). In contrast, activation of 4E-BP1 in adipose tissue did not prevent brown adipose tissue loss or alter the development of hepatic steatosis on a HFD (Figure 4, C and D, and Supplemental Figure 23). These data from HFD-fed mice with induced obesity and insulin resistance reinforce the concept that muscle-specific 4E-BP1 activation non–cell autonomously regulates fat metabolism.

Activation of 4E-BP1 in skeletal muscles preserved metabolic parameters in mice on HFD. Consistent with observations that *Tg-4EBP1mt-muscle* mice maintained insulin sensitivity and glucose homeostasis on a HFD, their metabolic rate was also maintained at a higher level (Supplemental Figure 24A). Moreover, HFD usually blocks RQ switch during the circadian cycle. *Tg-4EBP1mt-muscle* mice were protected from this (Supplemental Figure 24B). The PGC-1α targets associated with uncoupling, *Ucp2* and *Ucp3*, were further induced in the skeletal muscle of *Tg-4EBP1mt-muscle* mice, a finding that correlated with an enhanced metabolic rate (Supplemental Figure 25). Interestingly, we observed gender-dependent behaviors in *Tg-4EBP1mt-muscle* mice, as male *Tg-4EBP1mt-muscle* mice tended to eat less and female *Tg-4EBP1mt-muscle* mice tended to be more active (Supplemental Figure 26).

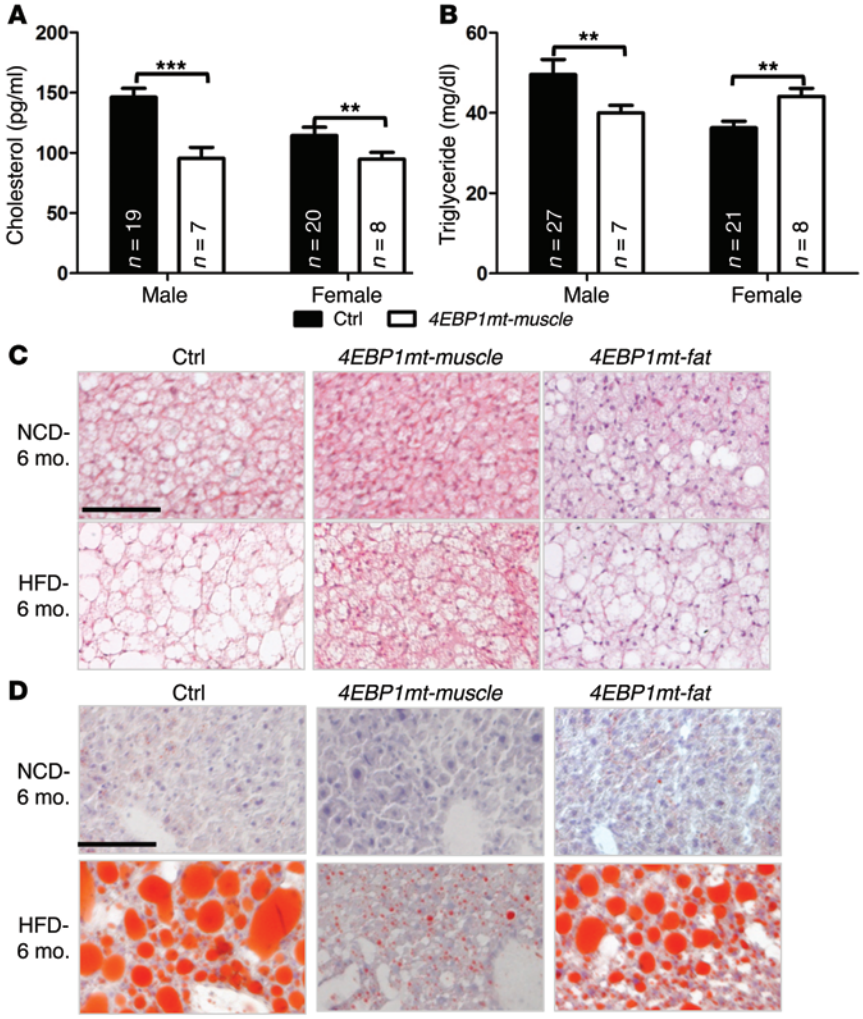

Figure 4. *Tg-4EBP1mt-muscle* mice have improved fat metabolism on HFD. (**A**) Cholesterol plasma values and (**B**) triglyceride plasma values from 6-month-old HFD-fed mice (the number of mice analyzed is indicated in bars). Representative images of (**C**) hematoxylin and eosin–stained brown adipose tissue sections and (**D**) Oil red O–stained liver sections from 6-month-old male mice. Scale bar: 100 μm. *P* values were assessed by a 2-way ANOVA. Bonferroni post-tests were used to compare replicate means by row. $^{**}P < 0.01$; $^{***}P < 0.001$. NCD, normal chow diet.

Tg-4EBP1mt-muscle mice are protected from age-induced metabolic decline. We have shown that activation of 4E-BP1 in skeletal muscle, instead of adipose tissue, suppresses fat metabolic dysfunction associated with HFD. Next, we investigated whether activation of 4E-BP1 in skeletal muscle also protects mice from age-induced metabolic dysfunction. The loss of skeletal muscle mass (sarcopenia) with age is associated with higher mortality in the elderly (51–53). Sarcopenia often leads to frailty, resulting in a decreased metabolic rate and increased risk of insulin resistance (54). We found that *Tg-4EBP1mt-muscle* mice, unlike their littermate control counterparts, preserved their muscle fiber size with advanced age (Figure 5, A and B; Supplemental Figure 27; and Supplemental Figure 28, B and C). In addition, whereas whole-body oxygen consumption declined in mice with age, *Tg-4EBP1mt-muscle* mice maintained higher levels of whole-body oxygen consumption (Figure 5C). RQ is usually reduced during aging in control mice (55), whereas 24-month-old aged *Tg-4EBP1mt-muscle* mice exhibited RQ levels comparable to those observed at 6 months of age (Supplemental Figure 29). Decreasing metabolic rate is usually associated with an increase in adiposity. We observed age-induced obesity in the control aging cohort, while *Tg-4EBP1mt-muscle* mice maintained body weight and adiposity during aging (Supplemental Figure 28). Because *Ucp1* expression was increased modestly in the brown fat pads of *Tg-4EBP1mt-muscle* mice (Supplemental Figure 8, B and C), we investigated the fate of brown fat in more detail. Loss of "browning" in brown adipose tissue has been correlated with increasing age (56, 57). At 17 months of age, we found marked white adipocyte infiltration in the brown fat pads of control mice. Strikingly, this infiltration was not apparent in *Tg-4EBP1mt-muscle* mouse brown adipose tissue at the same age (Figure 5D). Moreover, *Tg-4EBP1mt-muscle* mice have improved insulin sensitivity compared with that of aged control mice (Figure 5E). There was reduced a glucose tolerance, mainly due to increased insulin serum level, in aged male control mice (Figure 5, F and G), similar to previously reported observations (58). In contrast, *Tg-4EBP1mt-muscle* mice had insulin serum levels comparable to those of their younger counterparts and maintained improved glucose tolerance compared with that of aged controls. Thus, *Tg-4EBP1mt-muscle* mice are protected against age-induced metabolic decline both cell autonomously and non–cell autonomously.

Increased FGF21 expression from 4E-BP1–activated skeletal muscle. Activation of 4E-BP1 in skeletal muscle protects mice from either diet- or age-induced white adipose tissue accumulation and metabolic rate decline. When we screened for secreted myokines that might contribute to increased energy expenditure in 4E-BP1–activated skeletal muscle, we discovered that expression of *Fgf21* was significantly increased (Figure 6, A–C, and Supplemental Figure 30A). Correlated with this observation, the serum level of FGF21 was also higher in *Tg-4EBP1mt-muscle* mice (Figure 6D). In adipose tissue, FGF21 has been shown to regulate PPARγ activity, which contributes to enhanced metabolic activity in adipocytes (59). We observed increased expression of PPARγ in both white and brown adipose tissue (Figure 6E). As described above, white adipose tissue size was decreased and brown adipose tissue was preserved during HFD feeding or aging in *Tg-4EBP1mt-muscle* mice. We also observed decreased expression of genes involved in fatty acid and transgenic synthesis in white adipose tissue (Figure 6F), while there was increased expression in thermogenesis genes in brown adipose tissue (Figure 6G) on normal chow. A similar phenomenon was observed in *Tg-4EBP1mt-muscle* mouse liver, in which there was a reduction of SREBP1c expression, which regulated de novo lipogenesis and its target gene expression (Supplemental Figure 30, B

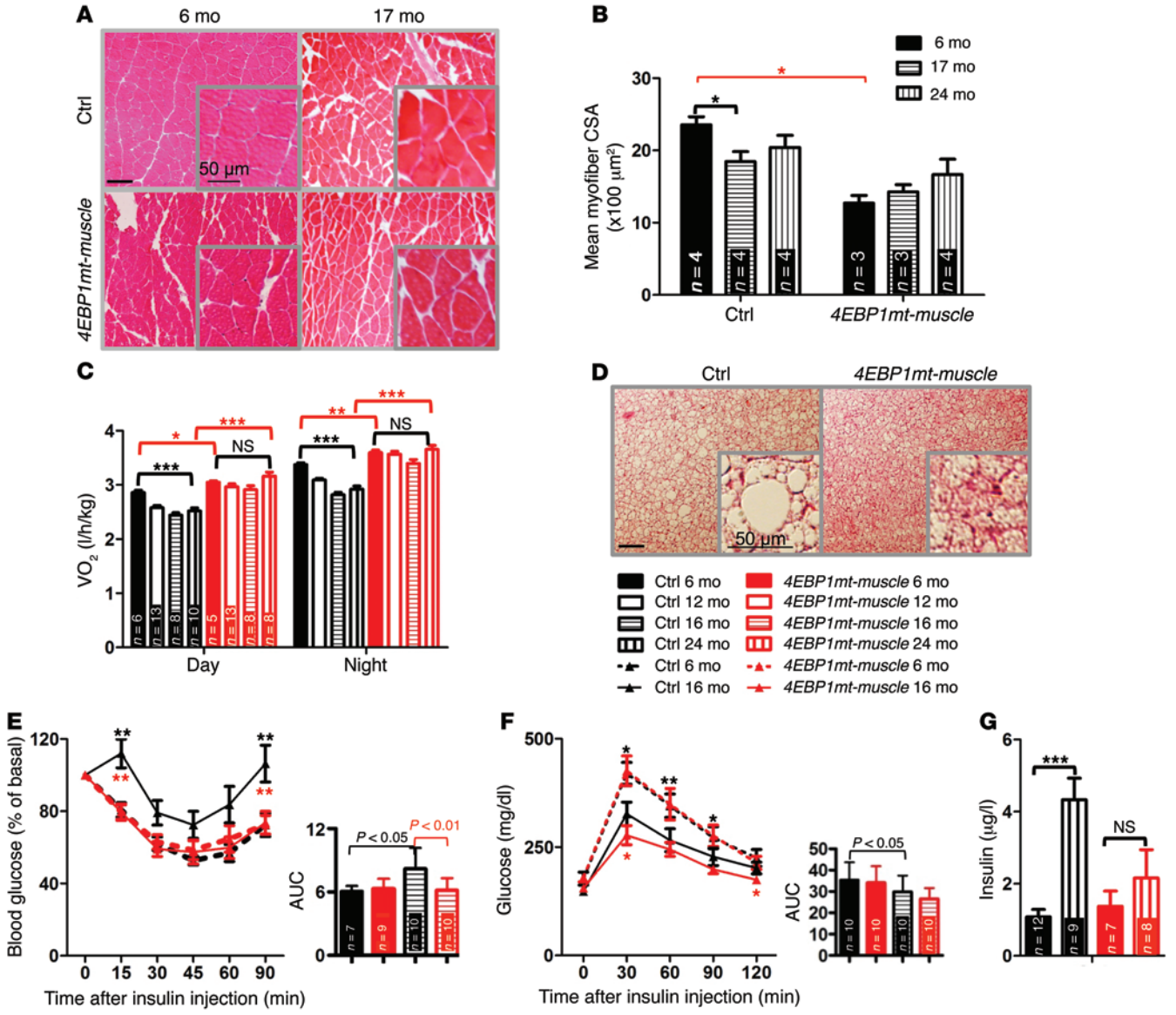

Figure 5. Activation of 4E-BP1 in mouse skeletal muscle protects mice from age-related metabolic decline. (**A**) Representative images of hematoxylin and eosin–stained quadriceps sections from male mice fed a normal chow diet. Scale bar: 100 μm; 50 μm (insets). (**B**) Analysis of the mean fiber cross-section area in quadriceps muscles (the number of mice analyzed is indicated in bars). *P* values were assessed by a 2-way ANOVA. Bonferroni post-tests were used to compare replicate means by row. (**C**) Oxygen consumption measured in a 3-day/night period in male mice at the indicated ages fed a normal chow diet (the number of mice analyzed is indicated in bars). *P* values were assessed by a 2-way ANOVA. Bonferroni post-tests were used to compare replicate means by row. (**D**) Representative images of hematoxylin and eosin–stained brown adipose sections from 17-month-old male mice fed a normal chow diet. Scale bar: 100 μm; 50 μm (insets). (**E**) Insulin challenge assay and (**F**) glucose tolerance assay in 6-hour–fasted male mice. Area under curve of the assay is plotted. *P* values were calculated by 1-tailed unpaired Student's *t* test. (**G**) Insulin level in 6-hour–fasted male mice fed a normal chow diet. *P* values were assessed by a 2-way ANOVA. Bonferroni post-tests were used to compare replicate means by row (the number of mice analyzed is indicated in bars). $^*P < 0.05$; $^{**}P < 0.01$; $^{***}P < 0.001$.

and C). Administration of FGF21 in obese or diabetic mice has been reported to increase β-oxidation in both adipose and liver tissue (59–62). There was no significant differential expression of β-oxidation genes in normal chow–fed *Tg-4EBP1mt-muscle* mice (Supplemental Figure 30C and Supplemental Figure 31, A and B); however, after 4 months of HFD feeding, we detected increased *Fgf21* expression in *Tg-4EBP1mt-muscle* mice (Supplemental Figure 31C) and markedly increased expression of β-oxidation genes in the skeletal muscle and white adipose tissue but not in liver (Supplemental Figure 31, D–F).

Induced 4E-BP1 activation in adult skeletal muscle retains increased metabolic rate. Since there is rapid skeletal muscle growth during the first week of postnatal development (63), activation of 4E-BP1 at this early stage might impair skeletal muscle growth and lead to a compromised metabolic phenotype. This raises the question of whether the phenotypes detected in the *Tg-4EBP1mt-muscle* mice were a result of differences during postnatal development or adulthood. To determine whether activation of 4E-BP1 in adult skeletal muscle directly triggers an enhanced metabolic rate without interfering with skeletal muscle development, we crossed *Tg-4EBP1mt*

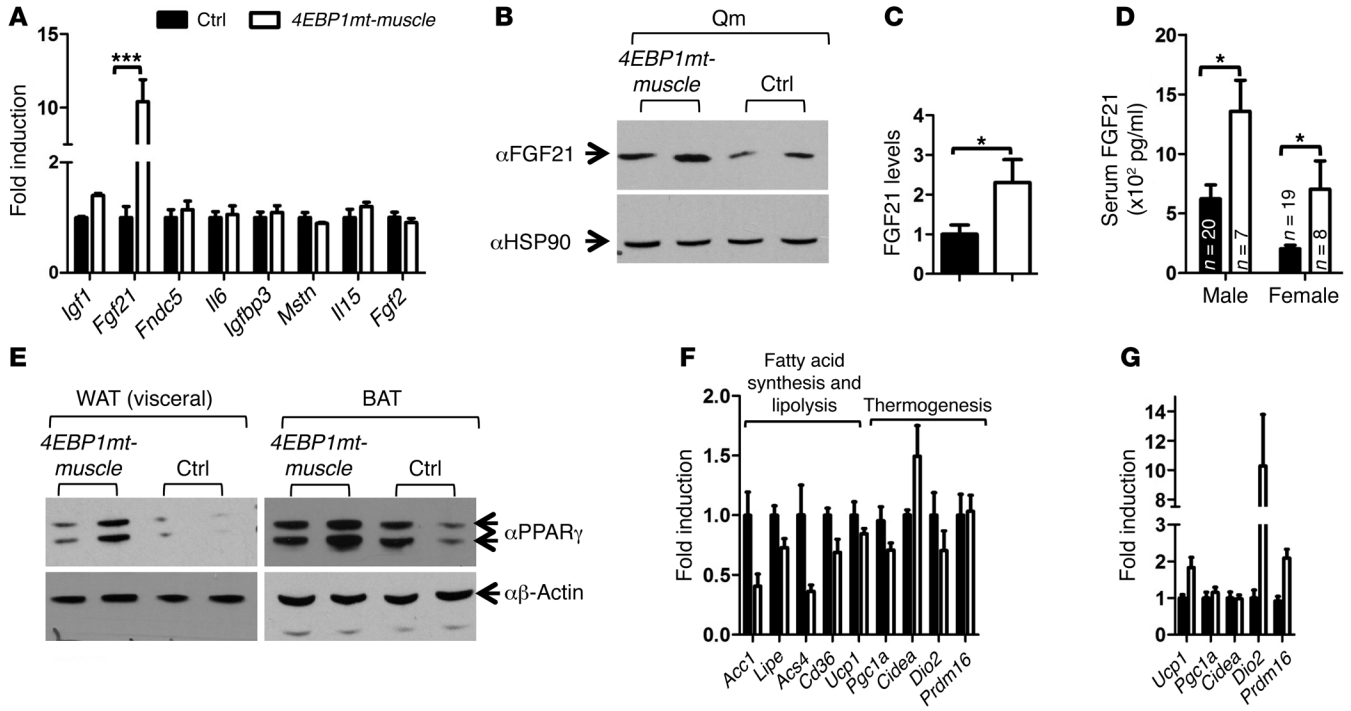

Figure 6. Increased FGF21 expression from 4E-BP1–activated skeletal muscle and altered expression of genes involved in fat metabolism in adipose and liver tissues. (**A**) RT-PCR quantification of myokine genes (n = 4) and (**B**) Western blots of quadriceps skeletal muscles (Qm) from 6-month-old male mice fed normal chow to detect FGF21 expression. (**C**) Quantification of FGF21 signaling from **B** normalized to the housekeeping gene, *HSP90*. *P* values were calculated by 1-tailed unpaired Student's *t* test. (**D**) Serum FGF21 level in fasted 6-month-old mice (the number of mice analyzed is indicated in bars). (**E**) Western blots of quadriceps muscles from 6-month-old male mice fed a normal chow diet to detect PPARγ expression in adipose tissues. WAT, white adipose tissue; BAT, brown adipose tissue. RT-PCR quantification of genes involved in fatty acid metabolism and thermogenesis in (**F**) white adipose tissue and (**G**) brown adipose tissue. *P* values from FGF21 ELISA and RT-PCR were assessed by 2-way ANOVA. Bonferroni post-tests were used to compare replicate means by row. $^*P < 0.05$; $^{***}P < 0.001$. RT-PCR samples were from n = 4 per genotype.

mice with *HSA-Cre-ER^{T2}* mice (64) to generate an inducible *4E-BP1* transgenic mouse model, *Tg-4EBP1mt-ER*, for adult skeletal muscle–specific activation. We induced transgenic *4E-BP1* expression at 2 months of age by daily injection of tamoxifen for 5 days, which activated *HSA-Cre-ER^{T2}* to excise the *loxP*-flanked STOP codon cassette of the *4E-BP1* transgenic allele (Figure 7A), and monitored body weight, lean mass, and metabolic rate at 4, 6, and 9 months of age. Western blot analysis of 4E-BP1 induction in mouse skeletal muscle confirmed the efficiency of *HSA-Cre-ER^{T2}*–mediated removal of the regulatory domain of the *4E-BP1* transgenic allele and induction of 4E-BP1 expression (Figure 7B). Induced 4E-BP1 activity in adult skeletal muscle clearly did not interfere with skeletal muscle mass buildup, as shown in body weight and lean mass measurements (Figure 7, C and D). Interestingly, *Tg-4EBP1mt-ER* mice, which have induced 4E-BP1 activity in adult skeletal muscle for 4 months, had an increased metabolic rate comparable to that of *Tg-4EBP1mt-muscle* mice at 6 months of age (Figure 7E) and correspondingly increased type I muscle gene expression in skeletal muscle (Supplemental Figure 32). Furthermore, there was induction of *Fgf21* expression in the skeletal muscle acutely activated by 4E-BP1. This increase in metabolic rate occurred without affecting skeletal muscle mass in *Tg-4EBP1mt-ER* mice, indicating that 4E-BP1 is directly involved in the regulation of oxidative metabolism and that FGF21 is likely mediating improved systemic metabolic homeostasis in response to activation of 4E-BP1.

Taken together, these results provide a comprehensive assessment of the consequences of enhanced mTORC1-nonresponsive 4E-BP1 activity in skeletal muscle and adipose tissue, leading us to conclude that activation of 4E-BP1 in skeletal muscle is a potent regulator of systemic whole-body metabolism. Muscle 4E-BP1 is also a promising therapeutic target to treat diet- and age-induced metabolic decline, since the acute activation of 4E-BP1 is sufficient to increase energy expenditure.

Discussion

Our data provide robust genetic evidence that the beneficial effects of mTOR-dependent regulation of 4E-BP1 activity are associated with skeletal muscle, rather than adipose tissue. Enhanced respiratory activity in *Tg-4EBP1mt-muscle* mice was apparent both in skeletal muscle and brown fat. While the former is likely due, at least in part, to enhanced PGC-1α activity, the non–cell autonomous effects on brown fat likely derive from increased FGF21 expression and secretion from skeletal muscle. While we cannot rule out a model whereby brown fat levels are enhanced due to secondary effects of reduced subcutaneous white fat to maintain body temperature, this seems unlikely since inactivation of *Rptor* in skeletal muscle also leads to white adipose tissue atrophy, without an increase in brown fat or any changes in body temperature regulation (17). Instead, we favor a model whereby (a) a myokine signal is transmitted from the skeletal muscle of *Tg-4EBP1mt-muscle* mice to brown fat or (b)

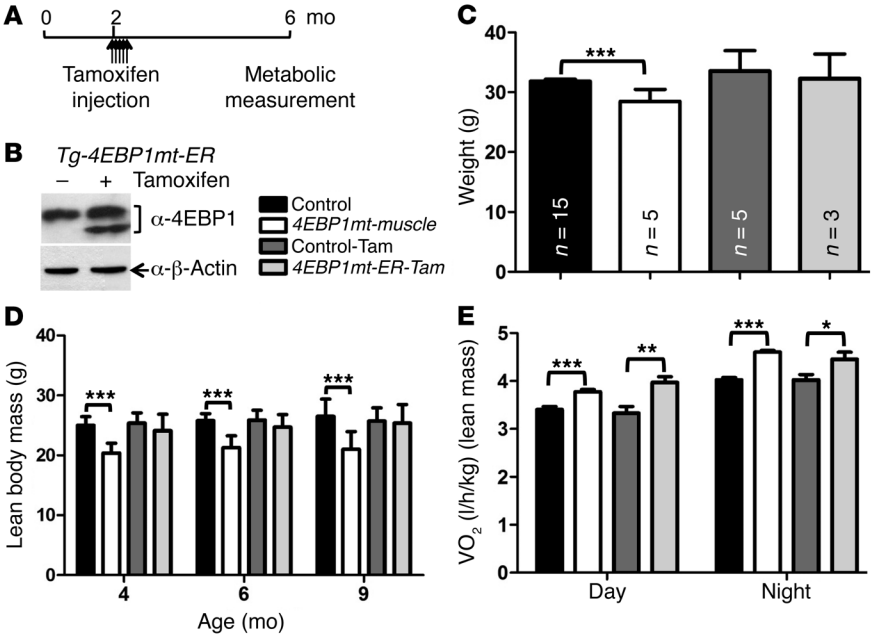

Figure 7. Induced 4E-BP1 activation in adult skeletal muscle retains the enhanced metabolic rate. (**A**) Schematic design of induced 4E-BP1 activation in adult skeletal muscle. (**B**) Western blot analysis of 4E-BP1 expression in quadriceps. Mice were harvested 2 days after the final injections of tamoxifen (TAM) at 2 months of age to check the induction level of 4E-BP1 expression. (**C**) Body weight measurement of male mice at 6 months of age (the number of mice analyzed is indicated in bars). (**D**) Lean mass measurement of male mice at the indicated ages (n = 3–5 per group). (**E**) Oxygen consumption measured in 3-day/night period in male mice at 6 months of age fed a normal chow diet (n = 3–5 per group). P values were assessed by a 2-way ANOVA. Bonferroni post-tests were used to compare replicate means by row. $^*P < 0.05$; $^{**}P < 0.01$; $^{***}P < 0.001$.

altered metabolism of skeletal muscle leads to metabolic changes that are interpreted differently by the heat-producing tissue.

Previously, the mTORC1 pathway was implicated in the regulation of adipogenesis, as inactivation of mTORC1 by RNAi knockdown of *Rptor* or treatment with rapamycin was found to reduce adipocyte differentiation (11). Conversely, preadipocytes lacking both *4E-BP1* and *4E-BP2* exhibit increased differentiation in vitro (28). Data from mice lacking *4e-bps* are conflicting, perhaps due to genetic background differences or tissue-specific effects of 4E-BP family members. Knockout of *4e-bps* results in a lean phenotype in the C57BL/6J background and, in contrast, leads to an obese phenotype in the BALB/c background (28, 65). In addition, *4e-bp1* single-knockout mice are lean (66), while *4e-bp1/2* double-knockout mice are obese (28). These differences may stem from different tissue-specific responses to 4E-BP family members in the regulation of metabolism. A similar phenomenon has been observed in mice chronically treated with rapamycin, which leads to hepatic inactivation of mTORC2, resulting in impaired fat metabolism and increased adiposity (67). Here, we show that 4E-BP1 activation is only beneficial in skeletal muscle, whereas the activation of 4E-BP1 in adipose tissue is deleterious upon HFD feeding. Thus, whole-body knockout of *4e-bps* or treatment with rapamycin may mask mTORC1-dependent regulation of adipogenesis and energy expenditure.

We performed our 4E-BP1 studies in transgenic mouse lines on the C57BL/6J background, as in previously published studies of genetically modified *Rptor* or *S6k1*$^{-/-}$ mice and in the rapamycin studies (5, 10, 11, 17, 68) to permit a direct comparison of metabolic phenotypes. Our data indicate that mTORC1-dependent regulation of 4E-BP1 activity in skeletal muscle, instead of adipose tissue, non–cell autonomously regulates fat metabolism in the context of aging and overnutrition.

Activation of 4E-BP1 in skeletal muscle induces autophagy, which in turn results in muscle atrophy. Similarly, whole-body deletion of *S6k1* also leads to muscle atrophy (69–71), perhaps secondary to AMPK activation. Whether autophagy genes are upregulated in *S6k1* knockout mice was not addressed. Both *Tg-4EBP-1mt-muscle* mice and *S6k1* knockout mice are lean and have high energy expenditure. Autophagy has been shown to be essential for maintaining favorable metabolic parameters in aging. For example, suppression of autophagy by knockout of *Atg7* (72) or activation of mTORC1 signaling (19) leads to an impaired metabolic rate and age-dependent myopathy, whereas transgenic activation of *Atg5* protects mice from age-induced metabolic decline and extends life span (73). It is possible that mild blunting of mTORC1 signaling in skeletal muscle leads to a sustained activation of autophagy. Our findings from the *Tg-4EBP1mt-muscle* mice thus indicate that elevated autophagy causes muscle atrophy and activates muscle metabolism, consequently stimulating fat metabolism and whole-body energy expenditure in the context of overnutrition and aging. However, a complete block of mTORC1 signaling leads to skeletal muscle deterioration and metabolic defects (16, 17).

Emerging evidence has identified 4E-BPs as key translational regulators mediating mTORC1-dependent signaling. Ribosome-profiling studies indicate that the translational targets of mTORC1 signaling are mainly mediated by 4E-BPs (74–76). Consistently, of the targets identified from previous studies (74, 75), *Foxo1* and *Akt1* were both increased in translation in skeletal muscle from *Tg-4EBP1mt-muscle* mice. Even though the previous ribosome-profiling studies were performed in cell lines, our data suggest similar results in vivo. Moreover, calorie restriction induces d4E-BP activation in the fly, which causes the selective translation of TOP mRNAs, indicating that enhanced mitochondrial biogenesis is a key underlying mechanism of 4E-BP–dependent life span extension (77). Here, we also found enhanced mitochondrial respiration with increased PGC-1α translation in 4E-BP1–activated skeletal muscle, suggesting that the beneficial effects of 4E-BP–regulated metabolic homeostasis are evolutionarily conserved.

Enhanced mTORC1 activity has been associated with glutamine addiction in cancer cells, as either reduced mTORC1 signaling or a depleted glutamine supply suppress tumor growth (48,

78–80). A recent study in a mouse model of Leigh syndrome found that repression of mTORC1 by rapamycin treatment in wild-type mice suppresses mitochondrial state III respiration rates in the presence of glutamate (47). Consistent with the current view that mTORC1 positively regulates glutamine metabolism, we observed that blunted mTORC1 activity via 4E-BP1 activation specifically suppresses glutamine metabolism, while enhancing the utilization of other TCA cycle substrates (81). Hence, 4E-BP1 activation may have therapeutic potential as a cancer treatment.

Reduced mTOR signaling mediated by rapamycin leads to a significant extension in life span and health span (5). The downstream effectors of these exciting phenotypes are yet to be fully resolved. Deletion of one mTORC1 target, *S6k1*, leads to life span extension, but to a lesser extent (10). The metabolic phenotypes reported here for *4EBP1mt-muscle* mice suggest mTORC1-dependent regulation of 4E-BP1 in skeletal muscle as another potential conduit through which these beneficial effects might be mediated upon aging.

Methods

Generation of tissue-specific 4E-BP1 transgenic mice and animals studies. A constitutively active mutant form (T37A and T46A) of human *4E-BP1* cDNA was placed downstream of a *loxP-GFP-3xstop-loxP* cassette under the control of a chicken β-actin promoter. The *GFP-stop* cassette prevents expression of the *4E-BP1* transgenic allele. Transgenic mice were crossed with mice expressing *Ckmm-Cre* (30) or a fatty acid–binding protein 4 promoter (*Fabp4-Cre*) (82) to induce *4E-BP1* transgene expression in skeletal muscle or adipose tissues, respectively. *HSA-Cre-ER^{T2}* mice (64) were bred with *Tg-4EBP1mt-ER* mice, harboring a constitutively active mutant form (T37A and T46A) of *4E-BP1* cDNA, to selectively induced expression of a mutant *4E-BP1* transgene under the control of the anti-estrogen tamoxifen administration. Control mice (single-transgenic mice: *HSA-Cre-ER^{T2}* mice or *Tg-4EBP1mt* mice) and *Tg-4EBP1mt-ER* mice were treated with 0.1 mg tamoxifen dissolved in corn oil for 5 consecutive days at 8 weeks of age. All mice used in this study were backcrossed to the C57BL6/J background for 5 generations, and littermate controls were used in the study. For the HFD-induced type 2 diabetes study, mice at 8 weeks of age were placed on either a standard laboratory rodent chow (2018, Harlan Teklad) or HFD (D12492, Research Diets) as indicated and monitored for 24 weeks.

Indirect calorimetric studies. Oxygen consumption, CO_2 production, volunteer home cage activity, and food and water intake were measured by open-flow respirometry (Sable systems).

Histological analysis and immunofluorescence. Tissue samples were either fixed in 4% paraformaldehyde solution in PBS before being embedded in paraffin or directly mounted in OCT before being stored at –80°C. After harvesting, muscle tissues were equilibrated in 30% sucrose (in PBS) for 2 to 3 hours and flash-frozen in liquid nitrogen–cooled isopentane. Morphology was examined in the hematoxylin and eosin–stained section. Oil red O staining was performed as previously described (83). Periodic acid–Schiff and Masson's trichrome staining were performed per the manufacturer's instructions (PAS Staining System, Sigma-Aldrich, and Masson's Trichrome Stain Kit, Dako). The size of muscle fibers and adipose cells was quantified in ImageJ. Results are shown as mean ± SEM of independent animals ($n \geq 4$). Muscle types were distinguished and quantified by immunofluorescence staining using antibodies against specific muscle type on snap frozen muscle sections (43). Primary antibodies were purchased from the Developmental Studies Hybridoma Bank (University of Iowa): BF-F8, SC-71, and BF-F3. Secondary antibodies were purchased from Invitrogen: Alexa Fluor 350 muIG2b, Alexa Fluor 488 muIG1, and Alexa Fluor 555 muIGM.

Treadmill endurance test. Control and transgenic mice were trained on a treadmill (18 meters per minute for 15 minutes) every other day for 1 week before the final test. For the treadmill running test, mice were run on a treadmill at a 5-degree inclination at a speed of 18 meters per minute. Endurance was measured by the total distance mice ran before exhaustion (n = 3~10 mice in each genetic group).

Blood lipids, glucose, and hormone analyses. Mouse blood was collected using the submandibular pouch technique. Sera were separated using Serum Separator Tubes (365956, BD). IGF-1 and growth hormone assays were performed in nonfasted mouse serum. The analysis of lipids, leptin, FGF21, and insulin profile was performed in sera collected from mice that were fasted for 6 hours. Triglyceride, free fatty acid, and cholesterol tests were purchased from Stanbio. The insulin test was purchased from Mercodia. The FGF21 ELISA was purchased from R&D Systems. All the assays followed the manufacturer's instructions. Leptin, IGF-1, and growth hormone tests were analyzed at the Diabetes, Endocrinology, and Metabolism Hormone Assay and Analytical Services Core at Vanderbilt University (n = 8~25 for each group).

Glucose and insulin tolerance assays. Glucose and insulin tolerance tests were performed on mice that were fasted for 6 hours. Glucose concentrations were determined with an Accu-Chek Advantage glucometer (Roche) in blood collected from the tail vein at the indicated time points. Insulin (0.75 U/kg for mice in the HFD group and 0.375 U/kg for mice in the normal chow diet group) or glucose (2 g/kg) was intraperitoneally injected into mice (n = 8 for each group).

RNA analyses. Total RNA was extracted from tissue using Trizol (Life Technologies) following the manufacturer's instructions (n = 4 for each group; 6-month-old male mice). An amount of 2 μg total RNA was reversely transcribed into cDNA by using the SuperScript III Reverse Transcription Kit (Invitrogen). Real-time PCR was performed in the Roche 480 iCycler PCR machine. Reactions were performed in triplicate, and relative amounts of cDNA were normalized to cyclophilin A (*Ppia*) or hypoxanthine guanine phosphoribosyl transferase (*Hprt*). qPCR primer sequences are listed in Supplemental Table 1.

Protein isolation and immunoblotting studies. Tissues were homogenized in cold SDS lysis buffer (50 mM Tris, pH 7.5, 70 mM urea, 250 mM sucrose, and 2% SDS) with Protease Inhibitor Cocktail (04693124001, Roche) and Phosphatase Inhibitor Cocktail II and III (P5726 and P0044, Sigma-Aldrich). 30 μg total protein was separated in 4% to 12% BT Precast Gel (NP0315, Invitrogen) or TGX Precast Gel (456-9033, Bio-Rad) and transferred to nitrocellulose membranes. Antibodies were from Cell Signaling (α-4E-BP1 [9452], α-eIF4E [2067], α-eIF4G [2469], α-AKT1 [4691], α-FOXO1 [2880], α-phospho-AKT Ser 473 [4058], α-LC3 [4108], α-PPARγ [2492], α-tubulin [3873], and α-β actin [4968]), abcam (α-FGF21 [ab171941], α-PGC1α [ab54481], α-UCP3 [ab3477], and α-SIRT4 [ab124521]), Santa Cruz Biotechnology Inc. (α-SREBP1 [SC-8984]), and Sigma-Aldrich (α-UCP1 [U6382]).

Cap-binding assay and immunoprecipitation. Tissues were homogenized in cold buffer A (10 mM Tris, pH 7.5, 150 mM KCl, 4 mM $MgCl_2$, and 1 mM EDTA and 1% NP-40) with Protease Inhibitor Cocktail (04693124001, Roche) and Phosphatase Inhibitor Cocktail II and III (P5726 and P0044, Sigma-Aldrich). For cap-binding assay, 1.2 mg tis-

sue lysate was incubated overnight at 4°C with 50 μl of the mRNA cap analogue m^7GTP-agarose (Jena Bioscience) in buffer A. The complex was wash once with buffer A. For immunoprecipitation, 1.2 mg tissue lysate was incubated overnight at 4°C with 5 μg eIF4E antibody or rabbit IgG in buffer A. 60 μl of the protein A/G plus-agarose (Santa Cruz) was added the next day and incubated at 4°C for 2 hours. The agarose beads were once washed in buffer A. Protein complex was eluted using 2× sample buffer and evaluated in Western blot.

Protein synthesis assay. A nonisotope-labeled protein synthesis assay was performed as previously described using the SUnSET method (84, 85). Puromycin (0.04 μM/g puromycin) was injected 30 minutes prior to harvesting. Protein was extracted and analyzed as stated above. Total protein was assessed with Coomassie blue staining, and puromycin-incorporated newly synthesized protein was detected by puromycin antibody (gift from Philippe Pierre, INSERM).

Isolation of intact mitochondria and oxygen consumption measurement. Isolation of mitochondria was performed using standard methods (86). Male mouse skeletal muscle mitochondria was isolated. Briefly, mouse skeletal muscles were dissected out and then rinsed twice in ice-cold CP1 buffer (100 mM KCl, 50 mM Tris-HCl, and 2 mM EGTA, pH 7.2, at 25°C). Tissues were quickly minced on an ice-cutting board and digested with 250 U/ 0.1 l protease type VIII, 0.5% BSA, 5 mM $MgCl_2$, and 1 mM ATP in CP1 buffer for 2.5 minutes at 4°C. After digestion, tissues were homogenized using a Dounce homogenizer, followed by an additional 3-minute incubation on ice, and centrifuged at 500 *g* at 4°C for 10 minutes. The supernatant was filtered through the 2 layers of muslin into the new centrifuge tube and centrifuged at 10,000 *g* at 4°C for 10 minutes, and the pellet was washed with ice-cold CP1 buffer twice. After final centrifugation at 10,000 *g* at 4°C for 10 minutes, the mitochondrial pellet was resuspended in CP1 buffer and immediately used for the oxygen consumption assay in XF24 Extracellular Flux Analyzer (Seahorse Bioscience) according to the manufacturer's instructions (87). Isolated muscle mitochondria (total 1.5 μg) was diluted in the mitochondrial assay solution (70 mM sucrose, 220 mM mannitol, 10 mM KH_2PO_4, 5 mM $MgCl_2$, 5 mM HEPES, 2 mM EGTA, and 0.2% BSA). State II respiration rate was measured in the presence of substrate (60 μM palmitoyl carnitine with 0.5 mM malate, 10 mM pyruvate with 0.5 mM malate, 5 mM glutamate with 0.5 mM malate, or 5 mM succinate with 0.002 mM rotenone). State III respiration rate was measured by adding 6 mM ADP in the presence of substrates. State IV(o) uncoupling rate was measured by adding 2.5 μg/ml oligomycin. The maximal respiration capacity was measured by adding 4 μM FCCP.

Mitochondrial DNA copy number measurement. Total DNA was extracted from tissue using lysis buffer with 100 mM Tris-HCl, pH 8.5, 5 mM EDTA, 0.2% SDS, 200 mM NaCl, and 0.1 mg/ml proteinase K. An amount of 0.2 μg total DNA was used for real-time PCR detection in the Roche 480 iCycler PCR machine. Reactions were performed in triplicate. Mitochondrial DNA was quantitated using *CoxII* gene and nuclear DNA was quantitated by β-actin.

Statistics. Unless otherwise stated, all results are expressed as mean ± SEM of *n* observations, and statistical differences among the groups were assessed by 2-way ANOVA. Bonferroni post-tests were used to compare replicate means by row. A unpaired and 1-tailed Student's *t* test was also used. A *P* value of more than 0.05 was considered significant.

Study approval. All experimental procedures involving animals in this study were reviewed and approved by the IACUC of Buck Institute for Research on Aging.

Acknowledgments

This study was supported by NIH grants R01AG033373 and R01AG035336 to B.K. Kennedy and R01 AG033082 to A.R. La Spada. B.K. Kennedy is also an Ellison Medical Foundation Senior Scholar in Aging. We thank Gary Scott, Pankaj Kapahi (Buck Institute for Research on Aging), and Matt Kaeberlein (University of Washington) for critical discussion, technical expertise, and reading of the manuscript. We also thank Philippe Pierre (INSERM, Marseille, France) for providing us with the anti-puromycin antibody and Pierre Chanbon (IGBMC, Illkirch, France) for providing us with *HSA-Cre-ER^{T2}* transgenic mice.

Address correspondence to: Albert R. La Spada, 2800 Torrey Pines Scenic Drive, La Jolla, California 92037-0642, USA. Phone: 858.246.0148; E-mail: alaspada@ucsd.edu. Or to: Brian Kennedy, Buck Institute for Research on Aging, 8001 Redwood Blvd., Novato, California 94945, USA. Phone: 415.209.2040; E-mail: bkennedy@buckinstitute.org.

1. Kaeberlein M. Longevity genomics across species. *Curr Genomics*. 2007;8(2):73–78.
2. Fontana L, Partridge L, Longo VD. Extending healthy life span — from yeast to humans. *Science*. 2010;328(5976):321–326.
3. Stanfel MN, Shamieh LS, Kaeberlein M, Kennedy BK. The TOR pathway comes of age. *Biochim Biophys Acta*. 2009;1790(10):1067–1074.
4. Johnson SC, Rabinovitch PS, Kaeberlein M. mTOR is a key modulator of ageing and age-related disease. *Nature*. 2013;493(7432):338–345.
5. Harrison DE, et al. Rapamycin fed late in life extends lifespan in genetically heterogeneous mice. *Nature*. 2009;460(7253):392–395.
6. Hay N, Sonenberg N. Upstream and downstream of mTOR. *Genes Dev*. 2004;18(16):1926–1945.
7. Ma XM, Blenis J. Molecular mechanisms of mTOR-mediated translational control. *Nat Rev Mol Cell Biol*. 2009;10(5):307–318.
8. Polak P, Hall MN. mTOR and the control of whole body metabolism. *Curr Opin Cell Biol*. 2009;21(2):209–218.
9. Um SH, D'Alessio D, Thomas G. Nutrient overload, insulin resistance, and ribosomal protein S6 kinase 1, S6K1. *Cell Metab*. 2006;3(6):393–402.
10. Selman C, et al. Ribosomal protein S6 kinase 1 signaling regulates mammalian life span. *Science*. 2009;326(5949):140–144.
11. Polak P, Cybulski N, Feige JN, Auwerx J, Ruegg MA, Hall MN. Adipose-specific knockout of raptor results in lean mice with enhanced mitochondrial respiration. *Cell Metab*. 2008;8(5):399–410.
12. Demontis F, Perrimon N. FOXO/4E-BP signaling in Drosophila muscles regulates organism-wide proteostasis during aging. *Cell*. 2010;143(5):813–825.
13. Bentzinger CF, et al. Differential response of skeletal muscles to mTORC1 signaling during atrophy and hypertrophy. *Skelet Muscle*. 2013;3(1):6.
14. Goodman CA, et al. A phosphatidylinositol 3-kinase/protein kinase B-independent activation of mammalian target of rapamycin signaling is sufficient to induce skeletal muscle hypertrophy. *Mol Biol Cell*. 2010;21(18):3258–3268.
15. Izumiya Y, et al. Fast/Glycolytic muscle fiber growth reduces fat mass and improves metabolic parameters in obese mice. *Cell Metab*. 2008;7(2):159–172.
16. Risson V, et al. Muscle inactivation of mTOR causes metabolic and dystrophin defects leading to severe myopathy. *J Cell Biol*. 2009;187(6):859–874.
17. Bentzinger CF, et al. Skeletal muscle-specific ablation of raptor, but not of rictor, causes metabolic changes and results in muscle dystrophy. *Cell Metab*. 2008;8(5):411–424.
18. Sandri M, et al. Signalling pathways regulating muscle mass in ageing skeletal muscle: the role of the IGF1-Akt-mTOR-FoxO pathway. *Biogerontology*. 2013;14(3):303–323.
19. Castets P, et al. Sustained activation of mTORC1 in skeletal muscle inhibits constitutive and

starvation-induced autophagy and causes a severe, late-onset myopathy. *Cell Metab*. 2013;17(5):731–744.
20. Cristancho AG, Lazar MA. Forming functional fat: a growing understanding of adipocyte differentiation. *Nat Rev Mol Cell Biol*. 2011;12(11):722–734.
21. Tseng YH, Cypess AM, Kahn CR. Cellular bioenergetics as a target for obesity therapy. *Nat Rev Drug Discov*. 2010;9(6):465–482.
22. Nader GA, Esser KA. Intracellular signaling specificity in skeletal muscle in response to different modes of exercise. *J Appl Physiol*. 2001;90(5):1936–1942.
23. van Wessel T, de Haan A, van der Laarse WJ, Jaspers RT. The muscle fiber type-fiber size paradox: hypertrophy or oxidative metabolism? *Eur J Appl Physiol*. 2010;110(4):665–694.
24. Wu J, Cohen P, Spiegelman BM. Adaptive thermogenesis in adipocytes: is beige the new brown? *Genes Dev*. 2013;27(3):234–250.
25. Lin J, et al. Transcriptional co-activator PGC-1 alpha drives the formation of slow-twitch muscle fibres. *Nature*. 2002;418(6899):797–801.
26. Wang YX, et al. Regulation of muscle fiber type and running endurance by PPARdelta. *PLoS Biol*. 2004;2(10):e294.
27. Gan Z, et al. Nuclear receptor/microRNA circuitry links muscle fiber type to energy metabolism. *J Clin Invest*. 2013;123(6):2564–2575.
28. Le Bacquer O, et al. Elevated sensitivity to diet-induced obesity and insulin resistance in mice lacking 4E-BP1 and 4E-BP2. *J Clin Invest*. 2007;117(2):387–396.
29. Gingras AC, et al. Regulation of 4E-BP1 phosphorylation: a novel two-step mechanism. *Genes Dev*. 1999;13(11):1422–1437.
30. Bruning JC, et al. A muscle-specific insulin receptor knockout exhibits features of the metabolic syndrome of NIDDM without altering glucose tolerance. *Mol Cell*. 1998;2(5):559–569.
31. Abel ED, et al. Adipose-selective targeting of the GLUT4 gene impairs insulin action in muscle and liver. *Nature*. 2001;409(6821):729–733.
32. Hsieh AC, et al. Genetic dissection of the oncogenic mTOR pathway reveals druggable addiction to translational control via 4EBP-eIF4E. *Cancer Cell*. 2010;17(3):249–261.
33. Puig O, Marr MT, Ruhf ML, Tjian R. Control of cell number by Drosophila FOXO: downstream and feedback regulation of the insulin receptor pathway. *Genes Dev*. 2003;17(16):2006–2020.
34. Bostrom P, et al. A PGC1-α-dependent myokine that drives brown-fat-like development of white fat and thermogenesis. *Nature*. 2012;481(7382):463–468.
35. Sandri M, et al. Foxo transcription factors induce the atrophy-related ubiquitin ligase atrogin-1 and cause skeletal muscle atrophy. *Cell*. 2004;117(3):399–412.
36. Goodman CA, Mayhew DL, Hornberger TA. Recent progress toward understanding the molecular mechanisms that regulate skeletal muscle mass. *Cell Signal*. 2011;23(12):1896–1906.
37. Kamei Y, et al. Skeletal muscle FOXO1 (FKHR) transgenic mice have less skeletal muscle mass, down-regulated Type I (slow twitch/red muscle) fiber genes, and impaired glycemic control. *J Biol Chem*. 2004;279(39):41114–41123.
38. Katewa SD, et al. Intramyocellular fatty-acid metabolism plays a critical role in mediating responses to dietary restriction in Drosophila melanogaster. *Cell Metab*. 2012;16(1):97–103.
39. Goodpaster BH, He J, Watkins S, Kelley DE. Skeletal muscle lipid content and insulin resistance: evidence for a paradox in endurance-trained athletes. *J Clin Endocrinol Metab*. 2001;86(12):5755–5761.
40. Amati F, et al. Skeletal muscle triglycerides, diacylglycerols, and ceramides in insulin resistance: another paradox in endurance-trained athletes? *Diabetes*. 2011;60(10):2588–2597.
41. Nadeau KJ, et al. Exercise training and calorie restriction increase SREBP-1 expression and intramuscular triglyceride in skeletal muscle. *Am J Physiol Endocrinol Metab*. 2006;291(1):E90–E98.
42. Schenk S, Horowitz JF. Acute exercise increases triglyceride synthesis in skeletal muscle and prevents fatty acid-induced insulin resistance. *J Clin Invest*. 2007;117(6):1690–1698.
43. Bloemberg D, Quadrilatero J. Rapid determination of myosin heavy chain expression in rat, mouse, and human skeletal muscle using multicolor immunofluorescence analysis. *PLoS One*. 2012;7(4):e35273.
44. Picard M, Hepple RT, Burelle Y. Mitochondrial functional specialization in glycolytic and oxidative muscle fibers: tailoring the organelle for optimal function. *Am J Physiol Cell Physiol*. 2012;302(4):C629–C641.
45. Lin J, Handschin C, Spiegelman BM. Metabolic control through the PGC-1 family of transcription coactivators. *Cell Metab*. 2005;1(6):361–370.
46. Scarpulla RC, Vega RB, Kelly DP. Transcriptional integration of mitochondrial biogenesis. *Trends Endocrinol Metab*. 2012;23(9):459–466.
47. Johnson SC, et al. mTOR inhibition alleviates mitochondrial disease in a mouse model of Leigh syndrome. *Science*. 2013;342(6165):1524–1528.
48. Csibi A, et al. The mTORC1 pathway stimulates glutamine metabolism and cell proliferation by repressing SIRT4. *Cell*. 2013;153(4):840–854.
49. Zhang J, et al. Dietary obesity-induced Egr-1 in adipocytes facilitates energy storage via suppression of FOXC2. *Sci Rep*. 2013;3:1476.
50. Wang YX, et al. Peroxisome-proliferator-activated receptor delta activates fat metabolism to prevent obesity. *Cell*. 2003;113(2):159–170.
51. Srikanthan P, Karlamangla AS. Muscle mass index as a predictor of longevity in older adults. *Am J Med*. 2014;127(6):547–553.
52. Chuang SY, Chang HY, Lee MS, Chia-Yu Chen R, Pan WH. Skeletal muscle mass and risk of death in an elderly population. *Nutr Metab Cardiovasc Dis*. 2014;24(7):784–791.
53. Janssen I, Ross R. Linking age-related changes in skeletal muscle mass and composition with metabolism and disease. *J Nutr Health Aging*. 2005;9(6):408–419.
54. Karakelides H, Nair KS. Sarcopenia of aging and its metabolic impact. *Curr Top Dev Biol*. 2005;68:123–148.
55. Houtkooper RH, et al. The metabolic footprint of aging in mice. *Sci Rep*. 2011;1:134.
56. Rogers NH, Landa A, Park S, Smith RG. Aging leads to a programmed loss of brown adipocytes in murine subcutaneous white adipose tissue. *Aging Cell*. 2012;11(6):1074–1083.
57. Cypess AM, et al. Identification and importance of brown adipose tissue in adult humans. *N Engl J Med*. 2009;360(15):1509–1517.
58. Leiter EH, Premdas F, Harrison DE, Lipson LG. Aging and glucose homeostasis in C57BL/6J male mice. *FASEB J*. 1988;2(12):2807–2811.
59. Dutchak PA, et al. Fibroblast growth factor-21 regulates PPARgamma activity and the antidiabetic actions of thiazolidinediones. *Cell*. 2012;148(3):556–567.
60. Emanuelli B, et al. Interplay between FGF21 and insulin action in the liver regulates metabolism. *J Clin Invest*. 2014;124(2):515–527.
61. Coskun T, et al. Fibroblast growth factor 21 corrects obesity in mice. *Endocrinology*. 2008;149(12):6018–6027.
62. Camporez JP, et al. Cellular mechanisms by which FGF21 improves insulin sensitivity in male mice. *Endocrinology*. 2013;154(9):3099–3109.
63. White RB, Bierinx AS, Gnocchi VF, Zammit PS. Dynamics of muscle fibre growth during postnatal mouse development. *BMC Dev Biol*. 2010;10:21.
64. Schuler M, Ali F, Metzger E, Chambon P, Metzger D. Temporally controlled targeted somatic mutagenesis in skeletal muscles of the mouse. *Genesis*. 2005;41(4):165–170.
65. Blackshear PJ, Stumpo DJ, Carballo E, Lawrence JC Jr. Disruption of the gene encoding the mitogen-regulated translational modulator PHAS-I in mice. *J Biol Chem*. 1997;272(50):31510–31514.
66. Tsukiyama-Kohara K, et al. Adipose tissue reduction in mice lacking the translational inhibitor 4E-BP1. *Nat Med*. 2001;7(10):1128–1132.
67. Lamming DW, et al. Rapamycin-induced insulin resistance is mediated by mTORC2 loss and uncoupled from longevity. *Science*. 2012;335(6076):1638–1643.
68. Um SH, et al. Absence of S6K1 protects against age- and diet-induced obesity while enhancing insulin sensitivity. *Nature*. 2004;431(7005):200–205.
69. Aguilar V, et al. S6 kinase deletion suppresses muscle growth adaptations to nutrient availability by activating AMP kinase. *Cell Metab*. 2007;5(6):476–487.
70. Pende M, et al. S6K1(–/–)/S6K2(–/–) mice exhibit perinatal lethality and rapamycin-sensitive 5′-terminal oligopyrimidine mRNA translation and reveal a mitogen-activated protein kinase-dependent S6 kinase pathway. *Mol Cell Biol*. 2004;24(8):3112–3124.
71. Ohanna M, et al. Atrophy of S6K1(–/–) skeletal muscle cells reveals distinct mTOR effectors for cell cycle and size control. *Nat Cell Biol*. 2005;7(3):286–294.
72. Masiero E, et al. Autophagy is required to maintain muscle mass. *Cell Metab*. 2009;10(6):507–515.
73. Pyo JO, et al. Overexpression of Atg5 in mice activates autophagy and extends lifespan. *Nat Commun*. 2013;4:2300.
74. Thoreen CC, Chantranupong L, Keys HR, Wang T, Gray NS, Sabatini DM. A unifying model for mTORC1-mediated regulation of mRNA translation. *Nature*. 2012;485(7396):109–113.
75. Hsieh AC, et al. The translational landscape of mTOR signalling steers cancer initiation and metastasis. *Nature*. 2012;485(7396):55–61.
76. Morita M, et al. mTORC1 controls mitochondrial

activity and biogenesis through 4E-BP-dependent translational regulation. *Cell Metab*. 2013;18(5):698–711.
77. Zid BM, et al. 4E-BP extends lifespan upon dietary restriction by enhancing mitochondrial activity in Drosophila. *Cell*. 2009;139(1):149–160.
78. Choo AY, et al. Glucose addiction of TSC null cells is caused by failed mTORC1-dependent balancing of metabolic demand with supply. *Mol Cell*. 2010;38(4):487–499.
79. Hensley CT, Wasti AT, DeBerardinis RJ. Glutamine and cancer: cell biology, physiology, and clinical opportunities. *J Clin Invest*. 2013;123(9):3678–3684.
80. Son J, et al. Glutamine supports pancreatic cancer growth through a KRAS-regulated metabolic pathway. *Nature*. 2013;496(7443):101–105.
81. Cornu M, Albert V, Hall MN. mTOR in aging, metabolism, and cancer. *Curr Opin Genet Dev*. 2013;23(1):53–62.
82. He W, et al. Adipose-specific peroxisome proliferator-activated receptor gamma knockout causes insulin resistance in fat and liver but not in muscle. *Proc Natl Acad Sci U S A*. 2003;100(26):15712–15717.
83. Mehlem A, Hagberg CE, Muhl L, Eriksson U, Falkevall A. Imaging of neutral lipids by oil red O for analyzing the metabolic status in health and disease. *Nat Protoc*. 2013;8(6):1149–1154.
84. Goodman CA, et al. Novel insights into the regulation of skeletal muscle protein synthesis as revealed by a new nonradioactive in vivo technique. *FASEB J*. 2011;25(3):1028–1039.
85. Schmidt EK, Clavarino G, Ceppi M, Pierre P. SUnSET, a nonradioactive method to monitor protein synthesis. *Nat Methods*. 2009;6(4):275–277.
86. Affourtit C, Quinlan CL, Brand MD. Measurement of proton leak and electron leak in isolated mitochondria. *Methods Mol Biol*. 2012;810:165–182.
87. Rogers GW, et al. High throughput microplate respiratory measurements using minimal quantities of isolated mitochondria. *PLoS One*. 2011;6(7):e21746.